The Knee 44 (2023) 130–141

Contents lists available at ScienceDirect

The Knee

journal homepage:

Dynamic CT scanning of the knee: Combining weight bearing with real-time motion acquisition

Luca Buzzatti [a,g,*], Benyameen Keelson [b,c,d], Joris Willem van der Voort [a], Lorenzo Segato [e], Thierry Scheerlinck [f], Savanah Héréus [a], Gert Van Gompel [b], Jef Vandemeulebroucke [c,d], Johan De Mey [b], Nico Buls [b], Erik Cattrysse [a], Ben Serrien [a]

[a] Vrije Universiteit Brussel (VUB), Experimental Anatomy Research Group (EXAN), Laarbeeklaan 103, 1090 Brussels, Belgium
[b] Vrije Universiteit Brussel (VUB), Universitair Ziekenhuis Brussel (UZ Brussel), Department of Radiology, Laarbeeklaan 101, 1090 Brussels, Belgium
[c] Vrije Universiteit Brussel (VUB), Department of Electronics and Informatics (ETRO), Pleinlaan 2, 1050 Brussel, Belgium
[d] imec, Kapeldreef 75, 3001 Leuven, Belgium
[e] Department of Neuroscience, Rehabilitation, Ophthalmology, Genetics, Maternal and Child Health, University of Genova, Campus of Savona, Italy
[f] Vrije Universiteit Brussel (VUB), Universitair Ziekenhuis Brussel (UZ Brussel), Department of Orthopaedic Surgery and Traumatology, Laarbeeklaan 101, 1090 Brussels, Belgium
[g] School of Allied Health, Anglia Ruskin University (ARU), Young Street, CB1 1PT Cambridge, UK

ARTICLE INFO

Article history:
Received 27 July 2022
Revised 14 June 2023
Accepted 24 July 2023

Keywords:
Dynamic CT
Weight-bearing
Knee kinematics
sEMG

ABSTRACT

Background: Imaging the lower limb during weight-bearing conditions is essential to acquire advanced functional joint information. The horizontal bed position of CT systems however hinders this process. The purpose of this study was to validate and test a device to simulate realistic knee weight-bearing motion in a horizontal position during dynamic CT acquisition and process the acquired images.
Methods: "Orthostatic squats" was compared to "Horizontal squats" on a device with loads between 35% and 55% of the body weight (%BW) in 20 healthy volunteers. Intraclass Correlation Coefficient (ICC), and standard error of measurement (SEM), were computed as measures of the reliability of curve kinematic and surface EMG (sEMG) data. Afterwards, the device was tested during dynamic CT acquisitions on three healthy volunteers and three patients with patellofemoral pain syndrome. The respective images were processed to extract Tibial-Tuberosity Trochlear-Groove distance, Bisect Offset and Lateral Patellar Tilt metrics.
Results: For sEMG, the highest average ICCs (SEM) of 0.80 (6.9), was found for the load corresponding to 42%BW. Kinematic analysis showed ICCs were the highest for loads of 42%BW during the eccentric phase (0.79–0.87) and from maximum flexion back to 20° (0.76). The device proved to be safe and reliable during the acquisition of dynamic CT images and the three metrics were computed, showing preliminary differences between healthy and pathological participants.
Conclusions: This device could simulate orthostatic squats in a horizontal position with good reliability. It also successfully provided dynamic CT scan images and kinematic parameters of healthy and pathological knees during weight-bearing movement.

Abbreviations: HS, horizontal squats; OS, orthostatic squats; sEMG, surface electromyography; MVC, Maximum Voluntary Contraction; %BW, body weight percentage; ICC, Intraclass Correlation Coefficient; SEM, Standard Error of Measurement; TTTG, tibial tuberosity-trochlear groove; BO, bisect offset; LPT, lateral patellar tilt; $CTDI_{vol}$, Volume Computed Tomography Dose Index; PFPS, patellofemoral pain syndrome.

* Corresponding author at: School of Allied Health, Anglia Ruskin University (ARU), Young Street, CB1 1PT Cambridge, UK.
E-mail address: Luca.Buzzatti@aru.ac.uk (L. Buzzatti).

https://doi.org/10.1016/j.knee.2023.07.014
0968-0160/

1. Introduction

Radiological imaging has an important role in the assessment of lower limb musculoskeletal conditions and several factors should be considered when doing such assessments. Firstly, images acquired in a supine position are missing important information about the effect that load has on the lower limb joints, and they do not sufficiently represent the kinematics during normal weight-bearing activities [1,2]; consequently, muscle activation should also be considered; thirdly, 3D images of the structures may provide more diagnostic information compared to 2D projections; lastly, dynamic acquisitions may provide additional information over static images as they are more representative of functional movements.

Several differences have been shown at the knee level when weight bearing (WB) was compared to non-weight bearing (NWB). Variations in joint alignment [3–5], estimation of morphological metrics [6], rotation [7], and displacement [8] are some of the changes reported between the two loading conditions. A further consequence of the patient's lower limb position is that moving from weight-bearing to non-weight bearing [9] or modifying muscle load [10,11] significantly affects muscle activation. Muscle contraction seems to have a substantial effect on knee kinematics (i.e. patella tracking) [12]; therefore, it should be an aspect to consider when investigating knee movement [13].

CT and MRI can acquire three-dimensional measurements, while conventional radiography is based on two-dimensional projections. The latter has been shown to be prone to error due to the variability in patient positioning. This leads to incorrect assessment of lower limb alignment, bony landmarks, and angle measurements on the knee [14–17] and foot [18,19]. Moreover, CT imaging appeared to be more sensitive and accurate for detecting osteophytes and subchondral cysts than conventional fixed-flexion radiography, which suffers from overlapping bony contours [20].

Finally, the lower limb is a dynamic structure of the human body. It would benefit from being investigated during movement and not in a static position [21]. It has been reported how dynamic images demonstrate the patellar tilt angle more accurately [22] and the reproduction of abnormal biomechanics of unstable joints with an increased risk of false negatives when static images are used [23,24].

One image modality that allows real-time 3D image acquisition with high temporal and spatial resolution is dynamic CT or 4DCT. It is performed on a wide beam or wide volume CT scanner, one of the latest CT hardware developments currently used for fast single-heartbeat cardiac imaging. This CT platform can also be employed for dynamic imaging of other structures over a longitudinal distance of up to 16 cm [25,26]. More recently, 4DCT has been used to investigate the dynamics of musculoskeletal structures. It enables the identification of small kinematic changes [27–30] has the potential to detect upper [31] and lower limb [32] pathologies, and it allows the evaluation of surgical outcomes [33,34].

Although several devices have been proposed to induce lower limb load during MRI [35–37] and CT [38,39] acquisition, no device is available that allows loaded lower limb motion during horizontal scanning. Moreover, all reported dynamic CT studies investigating lower limb pathologies have been performed in non-weight-bearing conditions [32].

Hence, this study aimed to validate and test a loading device to simulate realistic weight bearing in a horizontal position for acquisition during dynamic CT. A two-phase study was designed to validate and evaluate the applicability of such a device. In the first phase, Horizontal squats (HS) on the device (at different loads) to Orthostatic squats (OS) were compared. During the second phase, which served as the proof-of-concept stage, the device underwent testing on the CT scan by performing a dynamic CT acquisition of volunteers' knees. The acquired images were then subjected to post-processing to calculate three kinematic metrics: Tibial-Tuberosity Trochlear-Groove distance (TTTG), Bisect Offset (BO) and Lateral Patellar Tilt (LPT). These are metrics commonly used in radiology and orthopaedics to portray knee kinematics and patella tracking [40] during surgical planning [41,42].

2. Material and methods

2.1. Phase one

2.1.1. Participants

Twenty healthy adults (13 male and 7 female, average age 26 ± 6, BMI: 22.7 ± 2.0 kg/m^2) volunteered between November 2018 and January 2019 for this study. The study was approved by the ethics committee of the University Hospital (B.U.N 143201837451), and all subjects signed written informed consent.

2.1.2. Device

A wooden, low X-ray attenuating, custom-made weight-bearing device was constructed to simulate orthostatic squat movements in a horizontal position (Figure 1a, b, Figure 2). The device consisted of 3 parts: 1. A base structure fixed to

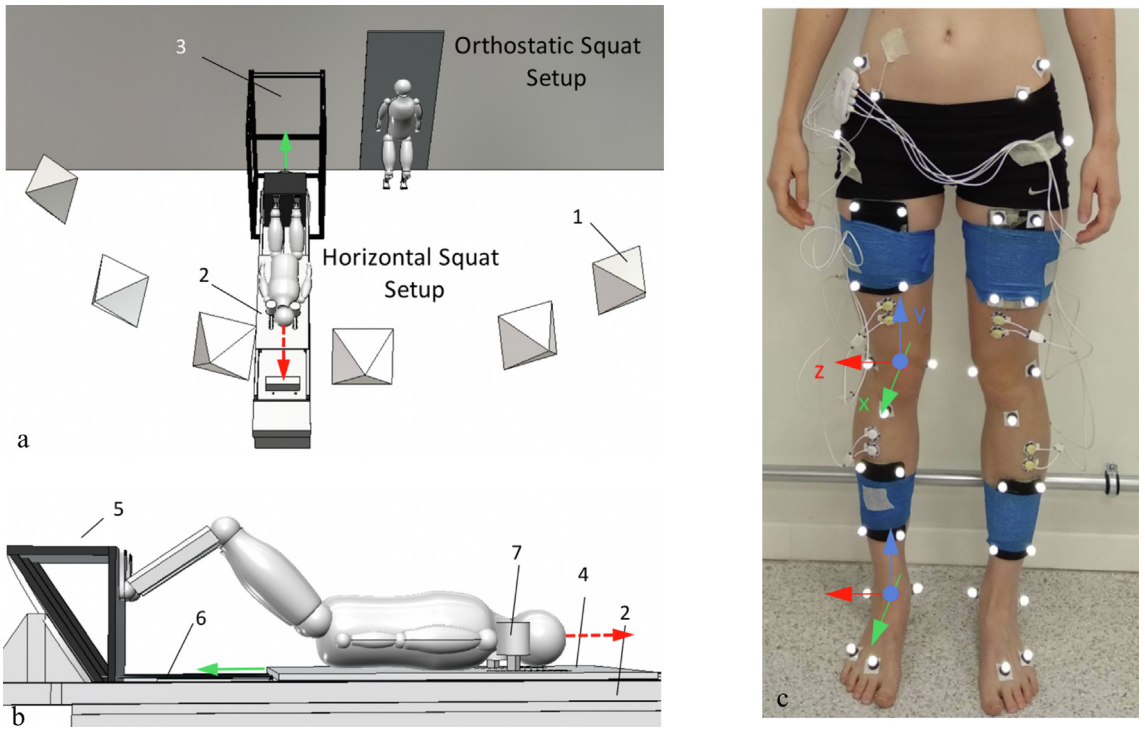

Figure 1. The study setup. **a**: The orthostatic and horizontal squat setup with the developed weight-bearing device. All movements were recorded with VICON infra-red cameras. **b**: Lateral view of the weight-bearing device. During concentric quadriceps contraction, the subject moves in the direction of the red-dashed arrow. The counteracting structure provides a constant counterforce in the direction of the green-solid arrow, which provides resistance in the concentric phase and brings the subjects back towards the platform in the eccentric phase. 1: VICON cameras; 2: base structure; 3: counteracting structure; 4: moving bed; 5: platform; 6: cable between the moving bed and the counteracting structure; 7: shoulder support. **c**: position of the reflective infra-red markers and sEMG electrodes on a subject. The arrows show the two reference frames' orientation to describe knee kinematics. Rotations about the z-axis represent knee flexion–extension movements, rotations about the y-axis represent internal-external rotation and rotations about the x-axis represent valgus-varus movements.

the CT scanner table and supplied, at one extremity, with a perpendicular foot platform. 2. A moving bed with two shoulder supports, rolling back- and forward over the base structure. 3. A counteracting loading structure connected to the moving bed and supplied with pulleys and weights (Figure 2c).

2.1.3. Setup

Two different tasks were considered: Horizontal squats (HS) on the device and Orthostatic squats (OS) (Figure 1a). While on the device, the subject pushed themselves away from the platform (knee extension). The counter-weight system acted similarly to gravity in the OS setting, bringing the subject back into a knee-flexion position. To make sure the two tasks were comparable a standardisation procedure was applied. To control trunk position, subjects were asked to perform the OS with the back minimally sliding up and down a smooth surface on the wall. Considering the importance of foot positioning [43], the contour of the device's platform was replicated on the floor using tape. The volunteers were asked to position their second toes on the top of the platform at an equal distance from the midline. The same foot position was replicated for the OS.

In both settings, a metronome set at 20 beats per minute, imposed the rhythm at which knee flexion–extension had to be performed. The two set-ups were placed close to each other so that the 6 cameras could capture both movements without repositioning them for each set-up. This allows consistency in the marker capture acquisition and eliminates possible calibration errors.

Maximum Voluntary Contraction (MVC) was recorded for each selected muscle according to Barbero et al. [44] before starting the experiment.

Figure 2. Knee in fully extended position (a), and maximum knee flexion achieved (b), counter-weight system (c).

Seven loads were investigated: 35, 37, 40, 42, 45, 50, and 55 percent of body weight (%BW). In a previous pilot experiment, it was observed that 35 %BW was perceived as much easier compared to a standing squat, while 55 %BW was perceived as much harder.

The subjects were asked to alternate one set (6 repetitions) of OS and one set (6 repetitions) of HS. In order to account for muscle fatigue, 2 minutes of rest before starting with a different load was allowed. The loads for the HS were randomly ordered for each subject and the subjects performed the same number of repetitions in both settings. A total of 42 OS and 42 HS were then evaluated. The high number of OS allowed us to accurately capture the variability of what has been used as a reference movement for our comparison.

2.1.4. Data collection and data processing

Three-dimensional trajectories of twenty infra-red retro-reflective markers (Figure 1c) were acquired with a 6-camera VICON MX F20 (VICON® Peak, Oxford, UK) optoelectronic motion capture system at a sampling frequency of 250 Hz. Two local reference frames based on marker coordinates were defined to estimate knee kinematics and axis orientation based on ISB guidelines [45] (Figure 1c). The reference frame of the thigh was centred on the midpoint between the two epicondyles, while the reference frame of the shank was centred between the two malleoli. Two orthogonal right-handed reference frames were constructed on each leg from the two centres. The z-axis pointed laterally (flexion–extension), the y-axis pointed cranially (internal-external rotation) and the x-axis pointed anteriorly (valgus-varus). The relative motion of the knee (R_{knee}) between a distal segment (R_{leg}) and proximal segment (R_{thigh}) for a chosen time point was computed as follows:

$$R_{knee} = R_{leg}R_{thigh}^{-1}$$

From this rotational matrix R_{knee}, Cardan angles for the knee joint were computed based on a ZYX decomposition sequence. Since an overall measure of the motion was needed to estimate the similarity between OS and HS, the Euclidian Norm ($\|d\| = \sqrt{X^2 + Y^2 + Z^2}$) was calculated from the three components and used for subsequent reliability calculations.

Surface electromyography (sEMG) was acquired on four different muscles (Rectus Femoris, Bicep Femoris, Tibialis Anterior and Gastrocnemius Lateralis) using a wireless 8 channels bioPLUX© unit (PLUX Wireless Biosignals S.A, Arruda dos Vinhos, Portugal) with a sampling frequency of 1000 Hz (Figure 1c). These four muscles were chosen to balance practicality and importance due to their activation during a squat.

The average maximum muscle activation for each muscle was calculated over the repetitions. The results of each muscle were then expressed as a percentage of the corresponding MVC (MVC%).

The first and last repetitions were excluded from the data analysis for both OS and HS to eliminate potential motion deviations at the initialisation and end of the cycle.

All data were processed with custom-made software developed in Python language (Python 3.7.0).

2.1.5. Statistical analysis

Statistical analysis was performed in Spyder and RStudio (R Foundation for Statistical Computing, Vienna, Austria).

The independent variables used in the statistical analysis were the average of the peaks of the four central repetitions for the sEMG (average maximum activation for each setup) and the average of the four kinematic curves (full squat cycle) for the kinematics.

To assess the similarity between the HS and OS approach for the sEMG and kinematics, the Intraclass Correlation Coefficient (ICC) and Standard Error of Measurement (SEM) were calculated as a measure of agreement. SEM was calculated as $SEM = SD\sqrt{1 - ICC}$, where SD is the Standard Deviation of the scores from all subjects determined from the ANOVA.

For the kinematics, as curve data (joint angle time series) were available, an integrated pointwise-index approach recommended by Pini et al. was followed for this study [46]. Average values were considered over the right and left leg, as a symmetrical movement was considered, and one single measure of reliability was needed for this study.

Continuous kinematic measurements were performed during the experiment. However, two portions of the movement were identified as relevant for examination to estimate which load was the most appropriate: the first 20° flexion, from 20° to maximum flexion, from maximum flexion to 20° of flexion, and the last 20° until full extension. It has been shown that the transition from full extension to early flexion (~20°) is the most critical for patients suffering from patellofemoral instability and pain [2,47–49]. The best bodyweight percentage was determined through visual inspection of the 95% confidence intervals (95% CI) [50].

2.2. Phase two – Proof of concept

2.2.1. Dynamic CT images acquisition

Three healthy male volunteers (age: 22, 53 and 26; BMI: 32.0, 30.6 and 24.7 kg/m^2) and three female patients (age: 39, 28 and 36; BMI: 27.1, 24.1 and 22.3 kg/m^2, NPRS at present: 4, 4 and 3), suffering from right patellofemoral pain syndrome for more than six months, participated in the second part of the study. As the device was ultimately designed to investigate patients, it was necessary also to verify whether its use would be feasible and not worsen participants' symptomatology compared to a functional test (standing squat). These subjects were part of a pilot study for a more extensive case-control study approved by the University Hospital's ethics committee (B.U.N 143201733617). All subjects signed informed consent. The same knee flexion–extension movement of the first phase of the validation study was replicated on the CT scanner (Figure 2 and Supplemental Video Material 1) using 42% BW as load.

A dynamic CT scan protocol was performed using a wide beam CT scanner (Revolution CT, GE Healthcare) with a 256x0.625 mm detector configuration to simultaneously acquire images of both knees. To maximise temporal resolution and reduce motion artifacts, images were acquired in continuous cardiac scanning mode (three cycles 0–300%, using a 30 bpm ECG simulation) instead of cine mode [51], with a 50 cm large field of view, 80 kVp, 50 mA, 16 cm collimation, 2.5 mm slice thickness, 0.28 s tube rotation and a total scanning time of 6.7 s for all subjects. 3D volumes were reconstructed (ASIR-V) with time intervals of 1.4 s, yielding 50 3D volumes. The effective dose was estimated using the National Cancer Institute's detailed voxel-based dosimetry model [34].

2.2.2. Image processing and metrics calculation

The automated multi-atlas multi-label segmentation approach proposed by Keelson et al. [52] was implemented to eliminate the need for manual segmentations of the femur and tibia. The image registration workflow used segmentation of the reference image (knee in full extension) as a mask to guide the pairwise registration step between the reference image and subsequent time points. This workflow also allows us to automatically compute kinematic parameters based on twelve bony landmarks previously selected on the reference image. These landmarks were identified as extreme portions of the bone. Their identification was made possible by cross-checking their location in the three planes (sagittal, frontal and horizontal) provided by the CT image viewer. This process was facilitated by the leg being aligned to the z-axis of the CT scan.

Three kinematic metrics were computed (Figure 3): the tibial-tuberosity tracheal-groove distance (TTTG), the bisect offset (BO), and the lateral patellar tilt (LPT). 30° of flexion was chosen as a cut-off for the analysis, as the first degrees of flexion and the last degrees of extension are the most valuable ranges to investigate pathologies such as patellar instability [9]. As this phase aimed to show proof-of-concept of the device and serve as a preliminary pilot for future more extensive studies, a graphical representation and comparison of the results was performed. No statistical analysis was considered to identify differences between healthy subjects and patients.

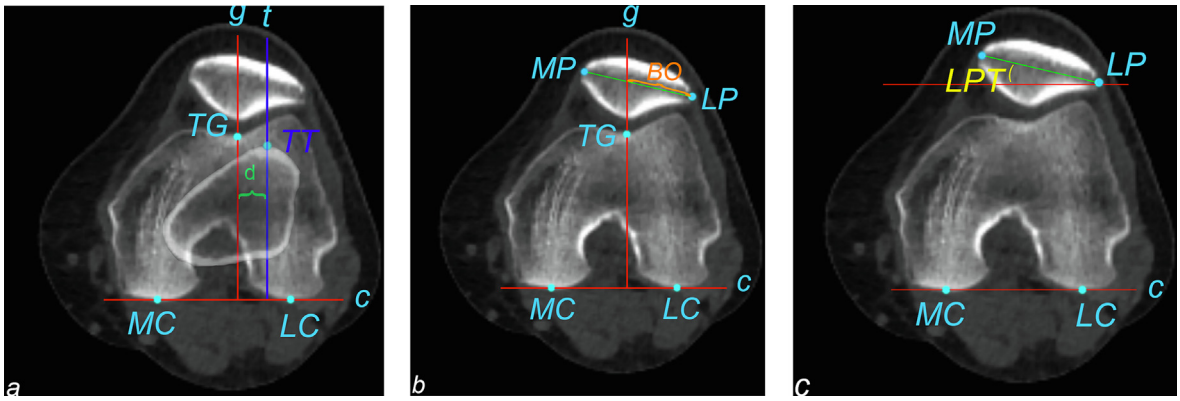

Figure 3. Kinematic metrics. The following bony landmarks were selected: the most posterior portion of the medial condyle (MC) and the lateral condyle (LC), the deepest point of the trochlear groove (TG), the most medial (MP) and lateral (LP) portion of the patella and the tibial tuberosity (TT). **(a)** The tibial-tuberosity tracheal-groove distance (TTTG) was defined as the distance (d) between the axis *g* and *t*. *g* is the axis passing through TG perpendicular to the axis passing through MC and LC (axis *c*). t is the axis passing through TT and perpendicular to the *c* axis. **(b)** The bisect offset (BO) was defined as the distance between LP and the intersection between *g* and the axis passing through MP and LP. This distance is expressed as a percentage (%) of the mediolateral size of the patella (distance between MP and LP). **(c)** The lateral patellar tilt (LPT) was defined as the angle (°) between *c* and the axis passing through MP and LP.

3. Results

3.1. sEMG results

The load of 42%BW showed the highest mean ICC of 0.80, followed by 45%BW with a mean ICC of 0.79, and 37%BW with a mean ICC of 0.78. The lower SEMs were reported for the central loads (40%,42%,45%), with the lowest at 42 %BW (6.9% MVC) (Table 1).

3.2. VICON motion analyses results

Figure 4 shows the results of SEM and ICC between the OS and HS from the kinematic analysis of the knee. During the eccentric phase, from 0° to 20°, all the %BWs showed similar SEM, while from 20° to maximum flexion (6.5° on average) a load of 42 %BW resulted in the lowest SEM (4.3°, 95% CI: 4.1–4.2). ICC was the highest for 42 %BW, reaching an average value of 0.79 (95% CI: 0.75–0.83) and 0.87 (95% CI: 0.86–0.88) for the first and second part of the eccentric phase, respectively. During the concentric phase, 42 %BW and 55 %BW showed the highest ICC (0.76), while 42 %BW showed the lowest SEM (5.5°, 95% CI: 5.2–5.7). By relying on 95%CI, in the last 20° of knee extension, no difference was seen among loads in terms of ICC and SEM.

3.3. Dynamic CT acquisition results

The device was successfully mounted on the CT bed and functioned as expected under load conditions. All participants reported that the device was comfortable and experienced no problems performing the movement on the CT. Moreover, the patients did not report an increase in their symptomatology. For each subject, a full flexion–extension motion was acquired during scanning. Figure 5 shows the acquired scan of one healthy subject from full knee extension to maximum flexion reached during the scanning procedure (Supplemental Video Material 2). The acquisition suffered from limited motion artifacts, and it was achieved with a low radiation dose ($CTDI_{vol}$ = 6.73 mGy, Effective dose = 0.02 mSv).

Figure 6 shows the three metrics extracted from the automated image processing workflow from 0° to 30° of knee flexion for healthy volunteers and patients. Patients showed TTTG, BO and LP ranging between 27.3 mm and 11.2 mm, between 109.5% and 62.9% and between 24.6° and 9.5° respectively. Healthy volunteers showed a range between 9.3 mm and 1.8 mm, 59.9% and 51.7% and 10.4° and 5.1° for the three respective metrics.

4. Discussion

This is the first study that estimates the similarity between an orthostatic squat and a horizontal loaded movement for medical image acquisition. The device for horizontal weight-bearing was reliable in reproducing similar knee kinematics and muscle activation compared to an orthostatic squat. A load of approximately 42 %BW resulted in the highest reliability and lowest error for a full flexion–extension cycle. Additionally, it was demonstrated how such a device could be implemented

Table 1
Intraclass Correlation Coefficient and Standard Error of Measurement between brackets, expressing reliability for rectified sEMG between orthostatic and horizontal squat for each body weight load (35–55%).

	35%		37%		40%		42%		45%		50%		55%	
	ICC	SEM	ICC	SEM	ICC	SEM	ICC	SEM	ICC	SEM	ICC	SEM	ICC	SEM
Rectus Femoris	0.82	8.3	0.87	7.7	0.80	8.4	0.84	8.1	0.86	7.1	0.80	10.0	0.85	8.7
Biceps Femoris	0.65	3.7	0.65	3.3	0.58	3.5	0.63	3.6	0.72	3.2	0.58	3.0	0.66	3.6
Tibialis Anterior	0.65	16.4	0.74	14.3	0.65	15.1	0.79	11.8	0.63	15.4	0.65	16.8	0.70	13.5
Gastrocnemius Lateralis	0.82	8.0	0.87	6.6	0.93	4.5	0.94	4.4	0.93	4.8	0.93	8.2	0.67	11.1
Mean	0.74	9.1	0.78	8.0	0.74	7.9	0.80	6.9	0.79	7.6	0.73	9.5	0.72	9.2

ICC: Intraclass Correlation Coefficient; SEM: Standard Error of Measurement.

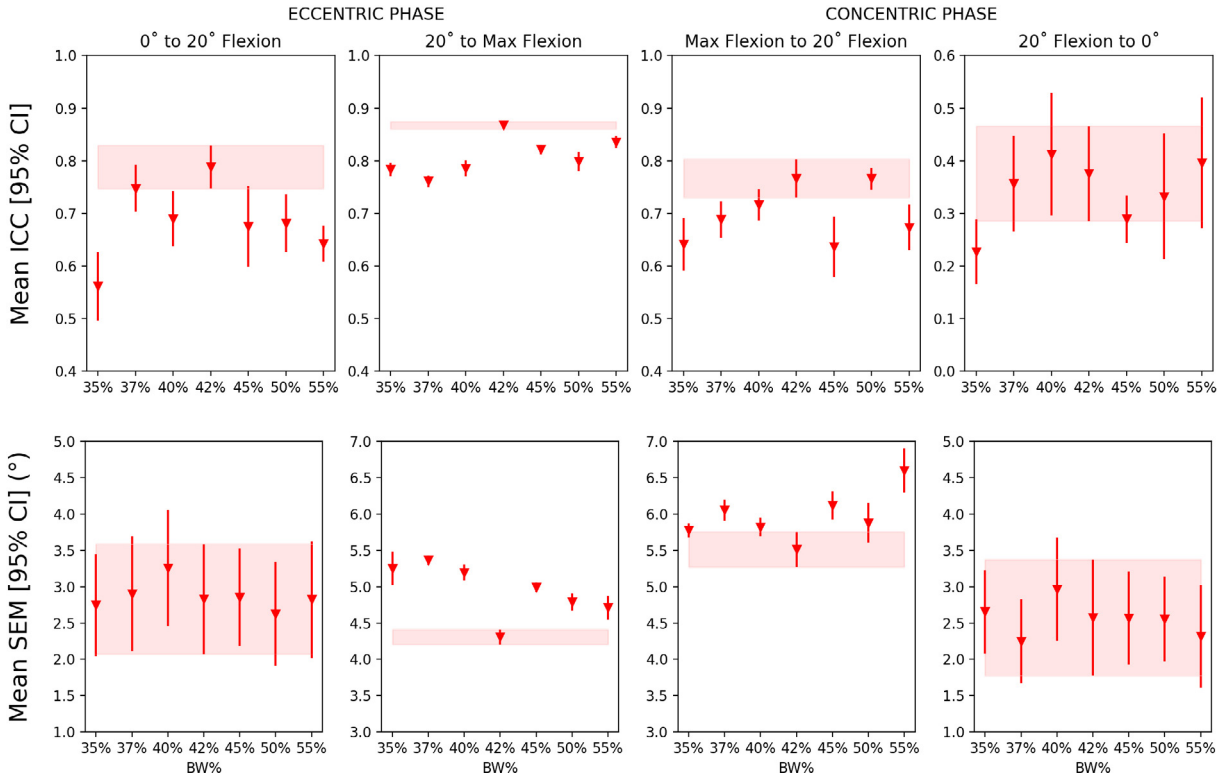

Figure 4. Mean Intraclass Correlation Coefficient (ICC) and Standard Error of Measurement (SEM, expressed in degrees) with corresponding 95% Confidence Intervals (CI) for the kinematic data. %BW: body-weight percentage. The red band represents the 95%CI of 42 %BW to highlight the comparisons with the other %BWs.

on a CT scanner, and dynamic CT acquisitions can be performed with healthy participants and patients. Such images can later be processed and qualitative (i.e., 3D bone morphology, visual dynamic bone interaction, presence and impact of OA) and quantitative information (i.e., Tibia-Tuberosity Trochlear-Groove, Bisect Offset, Lateral Patellar Tilt, 3D bone kinematics, surface contact) can be extracted. We could compute three kinematics metrics commonly used in orthopaedic surgery by implementing an automated image processing workflow with the dynamic CT images of the acquired knees.

The percentage of body weight applied in this study is similar to that of other devices (33%BW-50%BW) [37,39], indicating that similar body weight percentages have been used to simulate vertical load. However, due to its unique design with moving components, caution should be exercised when compared with other devices intended for static acquisitions.

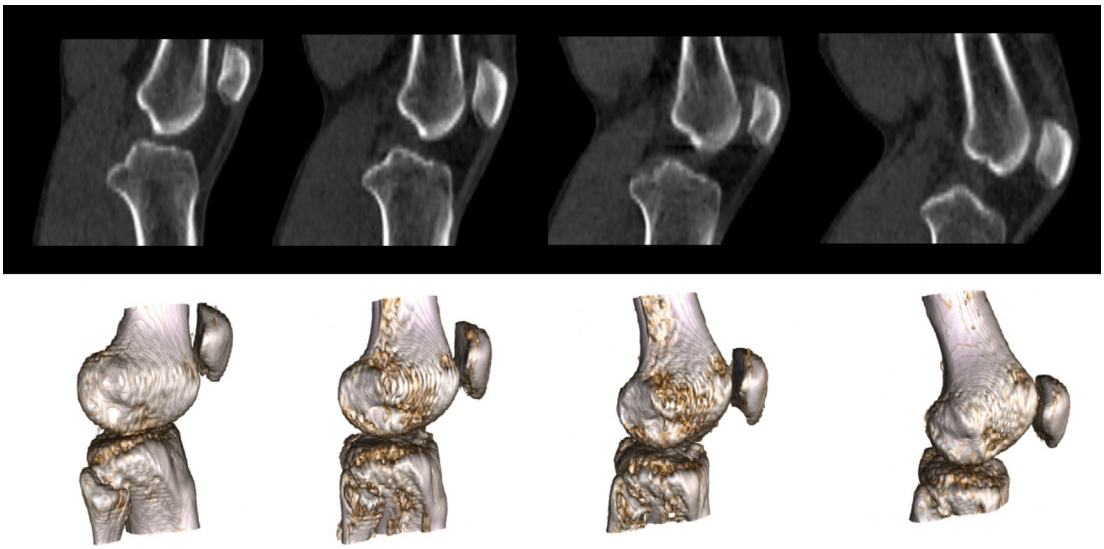

Figure 5. On the top: a sagittal CT view of the right knee from full extension to maximum flexion. On the bottom: a 3D volume rendering of the same images that can also be used to investigate joint morphology and bone interaction from a qualitative point of view.

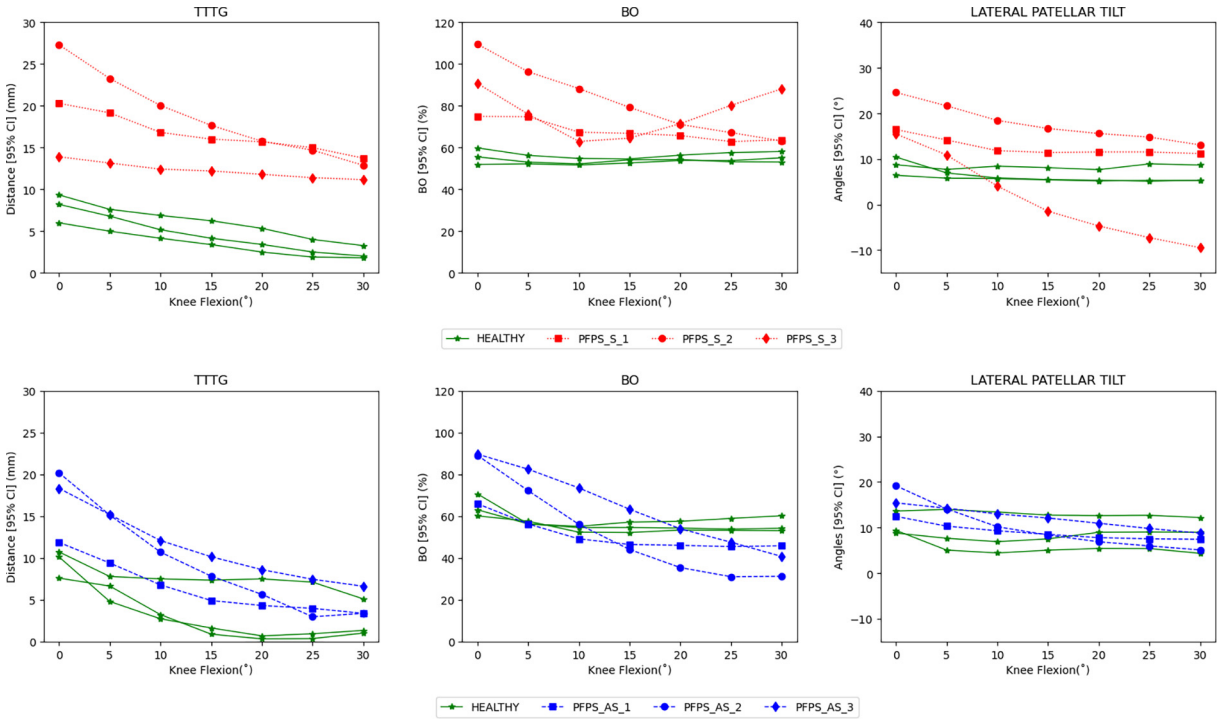

Figure 6. The top row represents the right knee of healthy subjects (green) and the right symptomatic (S) knees (red) of patients suffering from patellofemoral pain syndrome (PFPS). The bottom row represents the three left knees for healthy subjects (green) and the three asymptomatic (AS) knees (blue) of patients suffering from PFPS. TTTG: Tibial tuberosity-trochlear groove; BO: bisect offset.

In the proof-of-concept phase, the primary objective was to provide evidence that using the device on the CT machine is viable and that the subsequent image processing procedures can be effectively executed. This phase was successful in clearly depicting the kinematic curves. From the kinematic curves, two patterns could be observed: there were differences between painful knees, asymptomatic knees, and healthy subjects; TTTG and BO motion patterns of symptomatic subjects resemble those suffering from patellar dysfunctions, such as dislocation [53–55]. It is important to note that no clinical conclusions can be drawn due to the very small sample size and the characteristics (such as sex) of the participants. However, these findings present two potential areas of research that can build upon this proof-of-concept. Moreover, this is the first study to have captured and described orthopaedic metrics in a dynamic CT weight-bearing mode in subjects suffering from PFPS. Further studies with a larger sample size should explore differences between healthy and pathological patterns and between painful and asymptomatic knees. Additional validation of the device could include comparing weight-bearing and non-weight-bearing kinematics to compare differences and explore the benefits of one method over the other.

4.1. Clinical applications

Potentially several clinical applications using this device are possible. Different knee pathologies could be studied during weight-bearing acquisition. Anterior tibia translation, which is most pronounced between 20° and 45° of knee flexion [56] could be analysed to investigate anterior cruciate ligament (ACL) integrity or give valuable insight during pre-surgical planning and post-surgical evaluation. Patella instability and subluxation is another dynamic phenomenon, most predominant between 0° and 20–30° of knee flexion [8] that could be studied. The use of weight-bearing could also have an essential impact on orthopaedic metrics, such as the Tibia-Tuberosity Trochlear Groove distance, which are often used for surgical planning and that varies with the degree of knee flexion [53]. Evaluation of these parameters in non-weight-bearing conditions would exclude the stabilising effect of muscle contraction and could lead to inappropriate surgical indications. Dynamic CT could also investigate knee osteoarthritis and its impact on 3D joint space and kinematics. Standing CT is reliable and more precise than conventional radiography in evaluating joint space in patients with knee osteoarthritis [57]. The presented device in this study has the potential to achieve similar results with the added value of acquiring dynamic physiological motion at a lower radiation dose exposure compared to CBCT (0.02 mSv compared to 0.1 mSv, as reported by Segal et al. [20]). The effective dose associated with our imaging protocol is comparable to fixed-flexion knee radiographs (0.04–0.05 mSv for two lateral images and a bilateral posteroanterior view) [20].

This approach could also be extended to hip and ankle pathologies and offer the benefits of investigating them during dynamic functional load.

4.2. Limitations

The CT study was constrained by the field of view in the CT scanner (50 cm Ø × 16 cm), and correspondingly a limited knee flexion. However, as previously described, the first degrees of knee flexion seem the most relevant for several pathologies. Manufacturers are also currently working to enlarge the field of view up to 70 cm Ø and reduce tube rotation time to 0.23 s. This will allow a wider field of view and has the potential to decrease motion artifacts further.

A second limitation was the number of healthy subjects and patients included in our study. However, participants were recruited to verify that the device was able to function when mounted on the CT and that images could be acquired. Therefore, the limited numbers are in line with the aim of our study.

5. Conclusions

The current study showed high similarity (ICC > 0.75) of the knee joint kinematics and muscle activation between an orthostatic squat and a horizontal squat. 42%BW seems the most appropriate body-weight percentage to be used with this device configuration to better mimic an orthostatic squat. The implementation of the device on a wide-beam CT machine is also feasible with the possibility to acquire and process weight-bearing dynamic CT images of a moving knee joint in both healthy subjects and patients. Kinematic parameters of interest (i.e. TTTG, BO, LPT) can be computed from the image sequence and used to explore motion patterns. Compatibility with existing CT scanners and excellent reliability in reproducing a standing squat, make this device of potential interest for further validation studies and clinical applications.

Declaration of Competing Interest

The authors declare the following financial interests/personal relationships which may be considered as potential competing interests: 'The device has a pending patent (EP3875032A1) filed by the Vrije Universiteit Brussel and Luca Buzzatti, Benyameen Keelson, Thierry Scheerlinck, Gert Van Gompel, Jef Vandemeulebroucke, Johan De Mey, Nico Buls and Erik Cattrysse are listed as inventors.'.

Acknowledgements

The authors wish to thank Jessica Miller for the revision, correction and linguistic editing of the article.

The authors thank the Vrije Universiteit Brussel for the Interdisciplinary Research Project grant (IRP10, Karma4D) assigned to this project.

Appendix A. Supplementary material

Supplementary material to this article can be found online at https://doi.org/10.1016/j.knee.2023.07.014.

References

[1] Kim T-H, Sobti A, Lee S-H, Lee J-S, Oh K-J. The effects of weight-bearing conditions on patellofemoral indices in individuals without and with patellofemoral pain syndrome. Skeletal Radiol 2014;43:157–64. doi: https://doi.org/10.1007/s00256-013-1756-7.
[2] Draper CE, Besier TF, Fredericson M, Santos JM, Beaupre GS, Delp SL, et al. Differences in patellofemoral kinematics between weight-bearing and non-weight-bearing conditions in patients with patellofemoral pain. J Orthop Res 2011;29:312–7. doi: https://doi.org/10.1002/jor.21253.
[3] Jud L, Roth T, Roth T, Fürnstahl P, Vlachopoulos L, Sutter R, et al. The impact of limb loading and the measurement modality (2D versus 3D) on the measurement of the limb loading dependent lower extremity parameters. BMC Musculoskelet Disord 2020;:21. doi: https://doi.org/10.1186/S12891-020-03449-1.
[4] Marzo J, Kluczynski M, Notino A, Bisson L. Comparison of a novel weightbearing cone beam computed tomography scanner versus a conventional computed tomography scanner for measuring patellar instability. Orthop J Sports Med 2016;:4. doi: https://doi.org/10.1177/2325967116673560.
[5] Hirschmann A, Buck FM, Fucentese SF, Pfirrmann CWA. Upright CT of the knee: the effect of weight-bearing on joint alignment. Eur Radiol 2015;25:3398–404. doi: https://doi.org/10.1007/S00330-015-3756-6.
[6] Lullini G, Belvedere C, Busacca M, Moio A, Leardini A, Caravelli S, et al. Weight bearing versus conventional CT for the measurement of patellar alignment and stability in patients after surgical treatment for patellar recurrent dislocation. Radiol Med 2021;126:869–77. doi: https://doi.org/10.1007/S11547-021-01339-7.
[7] Johal P, Williams A, Wragg P, Hunt D, Gedroyc W. Tibio-femoral movement in the living knee. A study of weight bearing and non-weight bearing knee kinematics using "interventional" MRI. J Biomech 2005;38:269–76. doi: https://doi.org/10.1016/j.jbiomech.2004.02.008.
[8] Powers CM, Ward SR, Fredericson M, Guillet M, Shellock FG. Patellofemoral kinematics during weight-bearing and non-weight-bearing knee extension in persons with lateral subluxation of the patella: a preliminary study. J Orthop Sports Phys Ther 2003;33:677–85. doi: https://doi.org/10.2519/JOSPT.2003.33.11.677.
[9] Powers CM, Ho KY, Chen YJ, Souza RB, Farrokhi S. Patellofemoral joint stress during weight-bearing and non-weight-bearing quadriceps exercises. J Orthop Sports Phys Ther 2014;44:320–7. doi: https://doi.org/10.2519/JOSPT.2014.4936.
[10] Victor J, Labey L, Wong P, Innocenti B, Bellemans J. The influence of muscle load on tibiofemoral knee kinematics. J Orthop Res 2010;28:419–28. doi: https://doi.org/10.1002/JOR.21019.
[11] Wallace DA, Salem GJ, Salinas R, Powers CM. Patellofemoral joint kinetics while squatting with and without an external load. J Orthop Sports Phys Ther 2002;32:141–8. doi: https://doi.org/10.2519/JOSPT.2002.32.4.141.
[12] Witoński D, Góraj B. Patellar motion analyzed by kinematic and dynamic axial magnetic resonance imaging in patients with anterior knee pain syndrome. Arch Orthop Trauma Surg 1999;119:46–9. doi: https://doi.org/10.1007/S004020050353.
[13] Katchburian MV, Bull AMJ, Shih YF, Heatley FW, Amis AA. Measurement of patellar tracking: Assessment and analysis of the literature. Clin Orthop Relat Res 2003;412:241–59. doi: https://doi.org/10.1097/01.BLO.0000068767.86536.9A.
[14] Yoo HJ, Kim JE, Kim SC, Kim JS, Yang HJ, Kim TW, et al. Pitfalls in assessing limb alignment affected by rotation and flexion of the knee after total knee arthroplasty: Analysis using sagittal and coronal whole-body EOS radiography. Knee 2020;27:1551–9. doi: https://doi.org/10.1016/j.knee.2020.08.008.
[15] Khare R, Jaramaz B. Accuracy of leg alignment measurements from antero-posterior radiographs. Biomed Tech (Berl) 2017;62:315–20. doi: https://doi.org/10.1515/bmt-2015-0221.
[16] Hunt MA, Fowler PJ, Birmingham TB, Jenkyn TR, Giffin JR. Foot rotational effects on radiographic measures of lower limb alignment. Can J Surg 2006;49:401–6.
[17] Lonner JH, Laird MT, Stuchin SA. Effect of rotation and knee flexion on radiographic alignment in total knee arthroplasties. Clin Orthop Relat Res 1996:102–6. doi: https://doi.org/10.1097/00003086-199610000-00014.
[18] Baverel L, Brilhault J, Odri G, Boissard M, Lintz F. Influence of lower limb rotation on hindfoot alignment using a conventional two-dimensional radiographic technique. Foot Ankle Surg 2017;23:44–9. doi: https://doi.org/10.1016/j.fas.2016.02.003.
[19] Willauer P, Sangeorzan BJ, Whittaker EC, Shofer JB, Ledoux WR. The sensitivity of standard radiographic foot measures to misalignment. Foot Ankle Int 2014;35:1334–40. doi: https://doi.org/10.1177/1071100714549188.
[20] Segal NA, Nevitt MC, Lynch JA, Niu J, Torner JC, Guermazi A. Diagnostic performance of 3D standing CT imaging for detection of knee osteoarthritis features. Phys Sportsmed 2015;43:213–20. doi: https://doi.org/10.1080/00913847.2015.1074854.
[21] Carlson VR, Sheehan FT, Shen A, Yao L, Jackson JN, Boden BP. The relationship of static tibial tubercle-trochlear groove measurement and dynamic patellar tracking. Am J Sports Med 2017;45:1856–63. doi: https://doi.org/10.1177/0363546517700119.

[22] Muhle C, Brossmann J, Heller M. Kinematic CT and MR imaging of the patellofemoral joint. Eur Radiol 1999;9:508–18. doi: https://doi.org/10.1007/s003300050702.
[23] Rosa SB, Ewen PM, Doma K, Ferrer JFL, Grant A. Dynamic evaluation of patellofemoral instability: A clinical reality or just a research field? A literature review. Orthop Surg 2019;11:932–42. doi: https://doi.org/10.1111/os.12549.
[24] Freedman BR, Sheehan FT. Predicting three-dimensional patellofemoral kinematics from static imaging-based alignment measures. J Orthop Res 2013;31:441–7. doi: https://doi.org/10.1002/jor.22246.
[25] Tan KV, Thomas R, Hardcastle N, Pham D, Kron T, Foroudi F, et al. Predictors of respiratory-induced lung tumour motion measured on four-dimensional computed tomography. Clin Oncol (R Coll Radiol) 2015;27:197–204. doi: https://doi.org/10.1016/j.clon.2014.12.001.
[26] Schievano S, Capelli C, Young C, Lurz P, Nordmeyer J, Owens C, et al. Four-dimensional computed tomography: a method of assessing right ventricular outflow tract and pulmonary artery deformations throughout the cardiac cycle. Eur Radiol 2011;21:36–45. doi: https://doi.org/10.1007/s00330-010-1913-5.
[27] Buzzatti L, Keelson B, Apperloo J, Scheerlinck T, Baeyens J-P, Van Gompel G, et al. Four-dimensional CT as a valid approach to detect and quantify kinematic changes after selective ankle ligament sectioning. Sci Rep 2019;9:1291. doi: https://doi.org/10.1038/s41598-018-38101-5.
[28] Gondim Teixeira PA, Formery AS, Jacquot A, Lux G, Loiret I, Perez M, et al. Quantitative analysis of subtalar joint motion with 4D CT: Proof of concept with cadaveric and healthy subject evaluation. AJR Am J Roentgenol 2017;208:150–8. doi: https://doi.org/10.2214/ajr.16.16434.
[29] Tay SC, Primak AN, Fletcher JG, Schmidt B, Amrami KK, Berger RA, et al. Four-dimensional computed tomographic imaging in the wrist: proof of feasibility in a cadaveric model. Skeletal Radiol 2007;36:1163–9. doi: https://doi.org/10.1007/s00256-007-0374-7.
[30] Zhao K, Breighner R, Holmes 3rd D, Leng S, McCollough C, An KN. A technique for quantifying wrist motion using four-dimensional computed tomography: approach and validation. J Biomech Eng 2015:137. doi: https://doi.org/10.1115/1.4030405.
[31] White J, Couzens G, Jeffery C. The use of 4D-CT in assessing wrist kinematics and pathology: a narrative view. Bone Joint J 2019;101b:1325–30. doi: https://doi.org/10.1302/0301-620x.101b11.bjj-2019-0361.r1.
[32] Buzzatti L, Keelson B, Vanlauwe J, Buls N, de Mey J, Vandemeulebroucke J, et al. Evaluating lower limb kinematics and pathology with dynamic CT. Bone Joint J 2021;103-B:822–7. doi: https://doi.org/10.1302/0301-620X.103B5.BJJ-2020-1064.R2.
[33] Elias JJ, Carrino JA, Saranathan A, Guseila LM, Tanaka MJ, Cosgarea AJ. Variations in kinematics and function following patellar stabilization including tibial tuberosity realignment. Knee Surg Sports Traumatol Arthrosc 2014;22:2350–6. doi: https://doi.org/10.1007/s00167-014-2905-9.
[34] Gobbi RG, Demange MK, de Avila LFR, Araujo Filho JAB, Moreno RA, Gutierrez MA, et al. Patellar tracking after isolated medial patellofemoral ligament reconstruction: dynamic evaluation using computed tomography. Knee Surg Sports Traumatol Arthrosc 2017;25:3197–205. doi: https://doi.org/10.1007/s00167-016-4284-x.
[35] Silder A, Westphal CJ, Thelen DG. A magnetic resonance-compatible loading device for dynamically imaging shortening and lengthening muscle contraction mechanics. J Med Device 2009;:3. doi: https://doi.org/10.1115/1.3212559.
[36] Salsich GB, Ward SR, Terk MR, Powers CM. In vivo assessment of patellofemoral joint contact area in individuals who are pain free. Clin Orthop Relat Res 2003;417:277–84. doi: https://doi.org/10.1097/01.BLO.0000093024.56370.79.
[37] Jerban S, Chang EY, Du J. Magnetic resonance imaging (MRI) studies of Knee joint under mechanical loading: review. Magn Reson Imaging 2020;65:27. doi: https://doi.org/10.1016/J.MRI.2019.09.007.
[38] Zhang Y, Xu J, Wang X, Huang J, Zhang C, Chen L, et al. An in vivo study of hindfoot 3D kinetics in stage II posterior tibial tendon dysfunction (PTTD) flatfoot based on weight-bearing CT scan. Bone Joint Res 2013;2:255. doi: https://doi.org/10.1302/2046-3758.212.2000220.
[39] Ferràs-Tarragó J, Grau-Llopis E, Navarrete-Faubel E, Sánchez-González M, Vicent-Carsí V. An innovative weightbearing device for weightbearing 3-dimensional imaging for foot and ankle surgery preoperative planning. J Foot Ankle Surg 2021;60:1124–30. doi: https://doi.org/10.1053/J.JFAS.2020.06.032.
[40] Elias JJ, Soehnlen NT, Guseila LM, Cosgarea AJ. Dynamic tracking influenced by anatomy in patellar instability. Knee 2016;23:450–5. doi: https://doi.org/10.1016/J.KNEE.2016.01.021.
[41] S Z, D G. Preoperative planning of tibial tubercle medialisation according to the trochlear groove angle. Orthop Traumatol Surg Res 2019:105. doi: https://doi.org/10.1016/J.OTSR.2018.09.020.
[42] Fürmetz J, Daniel T, Sass J, Bergsträßer M, Degen N, Suero E, et al. Three-dimensional assessment of patellofemoral anatomy: Reliability and reference ranges. Knee 2021;29:271–9. doi: https://doi.org/10.1016/J.KNEE.2021.02.016.
[43] Signorile JF, Kacsik D, Perry A, Robertson B, Williams R, Lowensteyn I, et al. The effect of knee and foot position on the electromyographical activity of the superficial quadriceps. J Orthop Sports Phys Ther 1995;22:2–9. doi: https://doi.org/10.2519/JOSPT.1995.22.1.2.
[44] Barbero M, Rainoldi A, Merletti R. Atlas of muscle innervation zones. New York: Springer; 2012.
[45] Wu G, Siegler S, Allard P, Kirtley C, Leardini A, Rosenbaum D, et al. ISB recommendation on definitions of joint coordinate system of various joints for the reporting of human joint motion–part I: ankle, hip, and spine. Int Soc Biomech J Biomech 2002;35:543–8. doi: https://doi.org/10.1016/s0021-9290(01)00222-6.
[46] Pini A, Markstrom JL, Schelin L. Test-retest reliability measures for curve data: an overview with recommendations and supplementary code. Sports Biomech 2019:1–22. doi: https://doi.org/10.1080/14763141.2019.1655089.
[47] Leiprecht J, Mauch F, Huth J, Ambros LP, Best R. Weight-bearing MRI with a knee flexion angle of 20°: a study on additional MRI investigation modalities to support a more accurate understanding of patellofemoral instability. BMC Musculoskelet Disord 2021:22. doi: https://doi.org/10.1186/S12891-021-04733-4.
[48] Fulkerson JP. Diagnosis and treatment of patients with patellofemoral pain. Am J Sports Med 2002;30:447–56. doi: https://doi.org/10.1177/03635465020300032501.
[49] Pal S, Besier TF, Draper CE, Fredericson M, Gold GE, Beaupre GS, et al. Patellar tilt correlates with vastus lateralis: vastus medialis activation ratio in maltracking patellofemoral pain patients. J Orthop Res 2012;30:927–33. doi: https://doi.org/10.1002/JOR.22008.
[50] Cumming G. Inference by eye: reading the overlap of independent confidence intervals. Stat Med 2009;28:205–20. doi: https://doi.org/10.1002/SIM.3471.
[51] Keelson B, Buzzatti L, van Gompel G, Scheerlinck T, Hereus S, de Mey J, et al. The use of cardiac CT acquisition mode for dynamic musculoskeletal imaging. Phys Med 2022;104:75–84. doi: https://doi.org/10.1016/J.EJMP.2022.10.028.
[52] Keelson B, Buzzatti L, Ceranka J, Gutiérrez A, Battista S, Scheerlinck T, et al. Automated motion analysis of bony joint structures from dynamic computer tomography images: A multi-atlas approach. Diagnostics (Basel) 2021:11. doi: https://doi.org/10.3390/DIAGNOSTICS11112062.
[53] Tanaka MJ, Elias JJ, Williams AA, Carrino JA, Cosgarea AJ. Correlation between changes in tibial tuberosity-trochlear groove distance and patellar position during active knee extension on dynamic kinematic computed tomographic imaging. Arthroscopy 2015;31:1748–55. doi: https://doi.org/10.1016/j.arthro.2015.03.015.
[54] Tanaka MJ, Elias JJ, Williams AA, Demehri S, Cosgarea AJ. Characterization of patellar maltracking using dynamic kinematic CT imaging in patients with patellar instability. Knee Surg Sports Traumatol Arthrosc 2016;24:3634–41. doi: https://doi.org/10.1007/s00167-016-4216-9.

[55] Williams AA, Elias JJ, Tanaka MJ, Thawait GK, Demehri S, Carrino JA, et al. The relationship between tibial tuberosity-trochlear groove distance and abnormal patellar tracking in patients with unilateral patellar instability. Arthroscopy – J Arthroscopic Related Surg 2016;32:55–61. doi: https://doi.org/10.1016/j.arthro.2015.06.037.
[56] Dargel J, Gotter M, Mader K, Pennig D, Koebke J, Schmidt-Wiethoff R. Biomechanics of the anterior cruciate ligament and implications for surgical reconstruction. Strategies Trauma Limb Reconstr 2007;2:1–12. doi: https://doi.org/10.1007/S11751-007-0016-6.
[57] Segal NA, Bergin J, Kern A, Findlay C, Anderson DD. Test-retest reliability of tibiofemoral joint space width measurements made using a low-dose standing CT scanner. Skeletal Radiol 2017;46:217–22. doi: https://doi.org/10.1007/S00256-016-2539-8.